IEEE Access
Multidisciplinary | Rapid Review | Open Access Journal

Received January 21, 2020, accepted February 21, 2020, date of current version April 10, 2020.

Digital Object Identifier 10.1109/ACCESS.2020.2983516

Backhaul-Aware Trajectory Optimization of Fixed-Wing UAV-Mounted Base Station for Continuous Available Wireless Service

CHEN QIU, (Student Member, IEEE), ZHIQING WEI, (Member, IEEE), ZHIYONG FENG, (Senior Member, IEEE), AND PING ZHANG, (Fellow, IEEE)

Key Laboratory of Universal Wireless Communications, Ministry of Education, Beijing University of Posts and Telecommunications, Beijing 100876, China

Corresponding authors: Zhiqing Wei (weizhiqing@bupt.edu.cn) and Zhiyong Feng (fengzy@bupt.edu.cn)

This work was supported in part by the National Natural Science Foundation of China under Grant 61790553, and in part by the Beijing Natural Science Foundation under Grant L192031.

ABSTRACT Due to high mobility and flexibility, unmanned aerial vehicles (UAVs) have attracted significant attention from both academia and industry in wireless communications. Different types of UAVs are used for different wireless applications. However, there is a dilemma that no suitable approach is available to provide continuous available long-time wireless coverage from UAV-mounted base stations (UBSs) since rotary-wing UAVs require frequent energy replenishment while fixed-wing UAVs cannot hover at fixed locations. In this paper, the fixed-wing UBS is considered for providing continuous available wireless services to ground users with a novel dynamic resource allocation framework. In particular, the optimal resource allocations for both out-band and in-band wireless backhaul schemes are derived using convex optimization theory. Moreover, the sequential convex optimization method is used to obtain the energy-efficient trajectories. Finally, extensive simulation results are provided to verify the effectiveness of our proposed method. A comparison of out-band and in-band backhaul schemes is also provided.

INDEX TERMS Unmanned aerial vehicle, wireless backhaul, convex optimization.

I. INTRODUCTION

Unmanned aerial vehicles (UAVs) have attracted increasing attention in many areas. UAV-mounted base stations (UBSs) have emerged as a promising solution to provide wireless services to ground users [1], [2]. Compared to terrestrial communication systems, the high altitude of UBSs usually leads to a high probability of line-of-sight (LoS) links, which results in high-quality air-to-ground channels. Moreover, the UBSs are flexible that they can be easily reassigned and relocated [3].

The applications of UBSs are usually determined by the characteristics of different types of UAVs [4]. For example, the rotary-wing UAVs are equipped with propellers, which help them to hover at fixed locations. Therefore, the rotary-wing UBSs can provide continuous available wireless services and assist the cellular communication system in the service recovery scenario with partial infrastructure failure and in the scenario of coverage enhancement with extremely crowded users [5], [6]. However, the use of propellers requires high power consumption. Frequent energy replenishment is needed for rotary-wing UBSs. Hence, rotary-wing UAVs are not suitable for long time service provision.

On the contrary, fixed-wing UAVs have much longer flight duration since they typically consume much less power compared to rotary-wing UAVs [7]. However, fixed-wing UAVs are not capable of hovering at fixed locations. Therefore, existing studies have focused on leveraging the mobility of fixed-wing UBSs to improve transmit rate. For this purpose, only the users with strongest receiving signals are served at a given moment, while no service is provided to the rest users. Hence, the applications of fixed-wing UAVs are usually limited to delay-tolerant communications, such as data collection for sensor networks [8].

By comparing the characteristics of fixed-wing and rotary-wing UAVs, a dilemma is noticed that there is no suitable

The associate editor coordinating the review of this manuscript and approving it for publication was Wenchi Cheng.

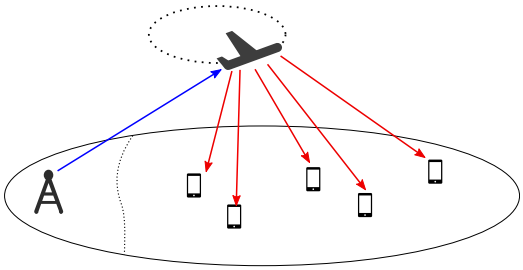

FIGURE 1. The fixed-wing UAV based network model, where the UBS provide the continuous available wireless services to ground users through the fronthaul links (red lines) and the GBS provides the wireless backhaul links (blue line) for the UBS.

approach to provide continuous available wireless services to ground users for a long time. To solve this problem, a novel design using fixed-wing UBS to provide continuous available wireless services is considered in this paper. To be specific, an energy-efficient joint resource allocation and trajectory design is studied for fixed-wing UBS.

Furthermore, as shown in Fig. 1, the UBS needs to connect with the ground base station (GBS) through a wireless backhaul link, where the GBS serves as a gateway to forward the user data to/from the core network. The out-band wireless backhaul scheme, where the fronthaul and backhaul links are operated in separated frequency bands, is usually considered in the existing works. On the other hand, the in-band wireless backhaul, which allows the backhaul links to be operated in the same band as the fronthaul links, has been considered in recent works to improve spectrum utilization [9], [10]. Based on the wireless backhaul schemes, the corresponding joint trajectory and resource allocation designs are discussed and analyzed in this paper.

A. RELATED WORKS

As mentioned above, the rotary-wing UBS can act as a static aerial base station. Several works have studied the placement optimization of UBS to improve network performance. For example, the optimal altitude that maximizes the converge area was derived in [11]. The optimal location of UBS to serve the maximum number of users was obtained in [12] by solving a mixed-integer nonlinear optimization problem.

Moreover, multiple-UBS placement has also been considered to provide services to large areas. In [13], a successive multiple-UBS placement scheme based on geometric disk cover problem was designed. An energy-efficient multiple-UBS deployment method based on optimal transport theory was developed in [14]. As an extension of [14], an optimal user association with maximum hovering time constraints was proposed in [15].

Meanwhile, some works considered wireless backhaul in the rotary-wing UBS deployment problems. To maximize the overall reliability of both fronthaul and backhaul links, an optimal altitude was derived in [16]. In [9], the overall spectrum efficiency was optimized by adjusting the altitude of UBS. In order to achieve the required network capability, a "working zoom" was derived and then used as a constraint for UBS placement problem in [17]. A multiple UBS placement problem with joint fronthaul and backhaul resource allocation was solved using convex optimization method in [18].

Although the fixed-wing UBSs can not hover at fixed locations, they can fly toward the target users to reduce transmission distances. As demonstrated in [19], the mobility of base stations have significant impact on the network capacity. In [4], with a given trajectory, a variable-rate protocol that can reduce the outage probability and improve the achievable information rate was developed to relay data between two ground stations. In a similar point-to-point relaying system, a joint trajectory and power allocation design was proposed in [20], where a significant throughput gain was achieved.

The trajectory design for multiple users was studied in recent works. In [21], a joint trajectory and communication design with multiple UBSs and multiple users was proposed. By considering the energy harvesting from solar power, a joint 3D trajectory and resource allocation problem was studied in [22]. In [23], a secure energy-efficiency trajectory design that avoids the eavesdroppers was designed. The optimization problems in [21], [22] and [23] have used the long-term throughput as the objective function or as a constraint. Therefore, the corresponding resource allocations would only serve the users with the strongest receiving signal at the given time slot, while no services are provided for the rest users. In other words, the ground users can only be served when the UBS is close to them, and they would suffer from significant delay when the UBS has flown away. This kind of resource allocation is not desirable in providing continuous available wireless services.

Motivated by the aforementioned delay problem, the trajectory design for delay-sensitive applications based on the rotary-wing UAVs was also considered in recent works. In [24], the tolerance for delay was considered as constraint in the throughput optimization problems. Another literature [25] considered the scenario that a fraction of user data is delay-sensitive. The interesting delay-throughput trade-off for rotary-wing UBS is demonstrated in both [25] and [24]. However, when the delay requirements are high, i.e., the tolerance for delay is 0 or the ratio of delay-sensitive user data is 1, the optimized trajectories in [24] and [25] become single points, which are not feasible trajectories for fixed-wing UAVs.

B. CONTRIBUTIONS

In this paper, the trajectory design and resource allocation of the fixed-wing UAV are jointly optimized to provide continuous available wireless services for ground users. The main contributions of this paper are three-fold.

1) We consider a practical problem of joint trajectory design and resource allocation for providing continuous available wireless services with a minimum rate

guarantee at every time slot, which has not been addressed in current studies.
2) We propose a framework to solve the energy-efficient trajectory design problem. In particular, the resource allocations for both out-band and in-band wireless backhaul schemes are derived in closed-form. Based on the optimal resource allocations, a sequential convex optimization framework that transforms the original problems into a sequence of convex optimization problems is developed.
3) Extensive simulations are conducted to prove the effectiveness of the proposed algorithms and provide a comparison between the out-band and in-band backhaul schemes.

The rest of this paper is organized as follows. Section II describes the system model. In Section III, the trajectory optimization problem of out-band backhaul scheme is formulated, and the corresponding sequential convex optimization method is developed. Similarly, the problem formulation and trajectory design for the in-band backhaul scheme are discussed in Section IV. The simulation results are provided in Section V to validate the performance of the proposed algorithm. Finally, Section VI concludes this paper.

II. SYSTEM MODEL

A. NETWORK MODEL

As shown in Fig. 1, we consider a geographic area in which a fixed-wing UBS is deployed to provide wireless services to a set of unserved ground users. In the meanwhile, a GBS is used to provide the wireless backhaul link for the UBS. The set of ground users is denoted as $\mathcal{M}$, and the locations of the ground users are given by $\boldsymbol{x}^{\text{user}} = \{x_j^{\text{user}} \in \mathbb{R}^2 | \forall j \in \mathcal{M}\}$. The location of the GBS is given by $x^{\text{gbs}} \in \mathbb{R}^2$. The goal of this paper is to optimize the UBS's trajectory to minimize the energy consumption while guarantees the minimum rate $R_{\min}$ for all users. The energy-efficient trajectory design can improve the endurance of the UBS and preserve the on-board energy for future assignments of different tasks. In particular, we focus on the optimization problem in a finite duration T, which can be divided into N discrete time slots. We assume that the time slot is small enough, and the projection of the UBS on ground at time slot $n \in \mathcal{N}$ can be approximated as a constant x_n, where $\mathcal{N} = \{0, 1, \ldots, N-1\}$. For convenience, the location of UBS at the end of T is denoted as x_N. Then, the trajectory can be denoted as a sequence of discrete points given by $\boldsymbol{x} = \{x_n \in \mathbb{R}^2 | \forall n \in \mathcal{N}^+\}$, where $\mathcal{N}^+ = \mathcal{N} \cup \{N\}$.

The UBS flies at a fixed altitude h, and the distance $d_{n,j}$ between user j and the UBS at time slot n is given by $d_{n,j} = \sqrt{\|x_n - x_j^{\text{user}}\|^2 + h^2}$, where $\|\cdot\|$ denotes the 2-norm. The distance between the GBS and the UBS at time slot n is given by $d_n^{\text{back}} = \sqrt{\|x^{\text{gbs}} - x_{n,j}\|^2 + h^2}$.

According to recent path loss measurements [26]–[28], the air-to-ground communication channels are dominated by the LoS links. In the 3GPP propagation model for UAV [29], the altitudes required for 100 % LoS channel in the Rural Macro scenario and the Urban Macro scenario are 40 m and 100 m, respectively. Since the high altitude is already required for UBS to avoid some obstructions from the ground, the altitude requirements for the LoS channel are reasonable. Moreover, the Rician fading model is commonly used to model the small scale fading in the LoS dominated channels, in which the Rician factor is used to characteristics the power ratio between the LoS signal component and the scattered signal component. Given the high altitude of UBS, the Rician factor is large enough, and the LoS channel model gives a reasonable approximation [30], [31]. Furthermore, by assuming the Doppler effect is compensated, the path loss can be modelled by the free space propagation. Let K be the transmit power of UBS, the received power of user j at time slot n is

$$S_{n,j} = \frac{K/(4\pi f/c)^2}{d_{n,j}^2},$$

where f is the carrier frequency, c is the speed of light. Then, the spectrum efficiency can be given as

$$E_{n,j} = \log\left(\frac{S_{n,j}}{\sigma} + 1\right),$$

where σ is the noise power. Similarly, the receiving power of the UBS at time slot n is

$$S_n^{\text{back}} = \frac{K^{\text{back}}/(4\pi f^{\text{back}}/c)^2}{|d_n^{\text{back}}|^2},$$

where K^{back} is the transmit power of GBS and f^{back} is the carrier frequency of backhaul. The corresponding spectrum efficiency of backhaul link is

$$E_n^{\text{back}} = \log\left(\frac{S_n^{\text{back}}}{\sigma} + 1\right).$$

B. RESOURCE ALLOCATION SCHEME

Since the wireless links are employed in the UBS backhaul, the backhaul resource allocation should be considered to avoid the interference between fronthaul and backhaul links. In particular, two resource allocation schemes are considered in this paper.

1) OUT-BAND BACKHAUL

The out-band backhaul scheme avoids the interference by assigning different frequency bands to the fronthaul and backhaul links. Without loss of generality, the time-division duplexing (TDD) with equally allocated uplink and downlink time slots is further assumed for both fronthaul and backhaul links. Since the frequency bands of fronthaul and backhaul links are isolated from each other, no fronthaul/backhaul time slot alignment is required for the out-band backhaul scheme.

2) IN-BAND BACKHAUL

To improve the spectrum utilization, the in-band backhaul scheme could be used to dynamically allocate the resources to fronthaul and backhaul links from a common frequency band.

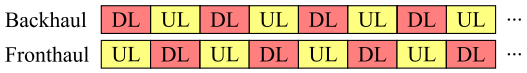

FIGURE 2. Reverse-TDD time slots configuration.

However, as a result of the band sharing, a carefully designed resource allocation is required. In particular, simultaneously transmitting and receiving should be avoided at the UBS to prevent self-interference. Assume that the TDD with equally allocated uplink/downlink time slots is used and the time slots of fronthaul and backhaul links are aligned, the reverse-TDD proposed in [32] is adopted. As illustrated in Fig. 2, the time slot configurations for uplink and downlink are reversed among fronthaul and backhaul. More specifically, the UBS is receiving data from both the GBS and the users in the first time slot. In the next time slot, the data collected from the users is forwarded to the GBS, and the data received from GBS is sent to the users. By repeating this process, self-interference is avoided.

C. ENERGY CONSUMPTION MODEL

In practice, the communication-related energy consumption is much smaller than the UBS's propulsion energy [33], [34]. Hence, the communication-related energy consumption is omitted in this paper. On the other hand, the energy consumption model developed in [35] is adopted to calculate the propulsion energy. Assuming that the velocity and acceleration are constant during a small time slot, the total propulsion energy consumption over the N time slots is

$$P=\delta\sum_{n\in\mathcal{N}}\left(c_1\|v_n\|^3+\frac{c_2}{\|v_n\|}\left(1+\frac{\|a_n\|^2-\frac{(a_n^{\mathsf{T}}v_n)^2}{\|v_n\|^2}}{g^2}\right)\right)+\Delta\kappa, \tag{1}$$

where $(\cdot)^{\mathsf{T}}$ indicates the transpose operation, $\delta=\frac{T}{N}$ is the length of each time slot, $a_n\in\mathbb{R}^2$ and $v_n\in\mathbb{R}^2$ are the acceleration and velocity of UBS in time slot n, c_1 and c_2 are two energy consumption parameters related to the UBS's weight, wing area, air density, and so forth, g is the gravitational acceleration, $\Delta\kappa=\frac{1}{2}m(\|v_N\|^2-\|v_0\|^2)$ is the change of the UBS's kinetic energy, v_N is the ending velocity, and m is the mass of the UBS.

D. REQUIREMENTS FOR TRAJECTORY DESIGN

The $\boldsymbol{v}=\{v_n|\forall n\in\mathcal{N}^+\}$ and $\boldsymbol{a}=\{a_n|\forall n\in\mathcal{N}\}$ mentioned above are respectively the time-varying velocity and acceleration vectors associated with the trajectory $\boldsymbol{x}$. Therefore, the relation between these variables can be expressed with the following discrete state-space equations

$$v_{n+1}=v_n+\delta a_n,\quad \forall n\in\mathcal{N}, \tag{2}$$

$$x_{n+1}=x_n+\delta v_n+\frac{\delta^2}{2}a_n,\quad \forall n\in\mathcal{N}. \tag{3}$$

Since the UBS flies at a fixed altitude, the velocity, acceleration and trajectory are considered within a two-dimensional horizontal plane.

The optimized trajectories should satisfy the following constraints that represent the physical velocity and acceleration limits of the UBS.

$$\|v_n\|\le v_{\max},\quad \forall n\in\mathcal{N}, \tag{4}$$

$$\|a_n\|\le a_{\max},\quad \forall n\in\mathcal{N}, \tag{5}$$

where $v_{\max}$ and $a_{\max}$ are the maximum velocity and acceleration, respectively.

Moreover, the UBS may abuse the kinetic energy to reduce the energy consumption. More specifically, the UBS will start the trajectory at a very high speed and end with a low speed that the change of kinetic energy becomes negative. Although the energy consumption within the target time period is reduced, this kind of trajectories is undesirable since the UBS should keep a reasonable velocity to reduce the overall energy consumption within the whole flying period. Therefore, the following constraint is adopted to prevent the abusing of kinetic energy $\Delta\kappa$.

$$\|v_0\|^2\le\|v_N\|^2. \tag{6}$$

It could be desirable that the trajectories start or end with given locations and velocities. For example, when the user distribution is diverged from the initial locations due to user mobility, it is desirable to use the current UBS location and velocity as starting points to design a new trajectory. However, the starting and ending point constraints are linear constraints, which can be easily handled by the convex optimization techniques used in this paper [36]. These starting/ending points constraints are omitted for brevity.

III. RESOURCE ALLOCATION AND TRAJECTORY DESIGN FOR OUT-BAND BACKHAUL SCHEME

To model the out-band backhaul scheme, the fronthaul bandwidth F and backhaul bandwidth B can be treat as two fixed parameters. Given the required rate $R_{\min}$, the optimization problem is formulated as

$$\underset{\boldsymbol{x},\boldsymbol{v},\boldsymbol{a},\boldsymbol{\beta}}{\text{minimize}}\ P \tag{7a}$$

$$\text{subject to}\ R_{\min}\le\beta_{n,j}E_{n,j},\quad \forall j\in\mathcal{M},\forall n\in\mathcal{N}^+, \tag{7b}$$

$$\sum_{j\in\mathcal{M}}\beta_{n,j}\le F,\quad \forall n\in\mathcal{N}^+, \tag{7c}$$

$$\sum_{j\in\mathcal{M}}\beta_{n,j}E_{n,j}\le E_n^{\text{back}}B,\quad \forall n\in\mathcal{N}^+, \tag{7d}$$

$$(2),\ (3),\ (4),\ (5)\ \text{and}\ (6),$$

where $\boldsymbol{\beta}=\{\beta_{n,j}|\forall j\in\mathcal{M},\forall n\in\mathcal{N}^+\}$ is the set of fronthaul bandwidth allocations for each user at each time slot. In this optimization problem, the constraints in (7b) guarantee that the required rate $R_{\min}$ is available for each user in each time slot. The constraints that the fronthaul resources allocated to users can not exceed the total fronthaul bandwidth are represented by (7c). The constraints in (7d) represent the requirements that the fronthaul rate should be accommodated by the backhaul link.

Since the objective function P and constraints (6), (7b) and (7d) are non-convex, (7) is a non-convex optimization problem and the global optimum is difficult to obtain. To tackle this problem, we firstly study the circular trajectory design as a special case. Based on the solution of the special case, an efficient iterative algorithm is proposed to solve (7).

A. CIRCULAR TRAJECTORY FOR OUT-BAND BACKHAUL

An empirical circular trajectory is considered in this subsection. It is assumed that the UBS flies at a constant velocity within the circular trajectory. Then, we have $\|v_n\| = v_{\text{cir}}, \forall n \in \mathcal{N}^+$, where v_{cir} is the constant velocity value. The magnitude of the centripetal acceleration required to maintain the circular trajectory is given as $\|a_n\| = \frac{v_{\text{cir}}^2}{r}, \forall n \in \mathcal{N}^+$, where r is the radius of the circular trajectory. Since the centripetal acceleration is always perpendicular to the velocity, we also have $a_n^{\mathrm{T}} v_n = 0$. By substituting the velocity and acceleration of the circular trajectory into the energy consumption model (1), the energy consumption of the circular trajectory is simplified as

$$P_{\text{cir}} = \delta N \left(\left(c_1 + \frac{c_2}{g^2 r^2} \right) v_{\text{cir}}^3 + \frac{c_2}{v_{\text{cir}}} \right), \tag{8}$$

where the change of kinetic energy is zero and omitted in (8). Since P_{cir} is a convex function of the velocity $v_{\text{cir}} \geq 0$, the optimal velocity can be obtained by solving the first-order optimality condition, i.e., $\partial_{v_{\text{cir}}} P_{\text{cir}} = 0$. The optimal velocity is given by

$$v_{\text{cir}}^{\star} = \sqrt[4]{\frac{c_2}{3\left(c_1 + \frac{c_2}{g^2 r^2}\right)}}. \tag{9}$$

By substituting $v_{\text{cir}}^{\star}$ into P_{cir}, the optimal energy consumption is derived as

$$P_{\text{cir}}^{\star} = \frac{4}{3} \delta N \sqrt[4]{3 c_2^3 \left(c_1 + \frac{c_2}{g^2 r^2} \right)}. \tag{10}$$

It can be checked that $P_{\text{cir}}^{\star}$ is a decreasing function of r, i.e., the minimizing of energy consumption is equivalent to obtain the maximum radius. To this end, a simplification of constraints (7b), (7d) and (7c) is studied. Notice that the max-min user rate $R^{\text{out}}(x_n)$ can be defined as the optimal objective value of the following optimization problem.

$$R^{\text{out}}(x_n) = \begin{cases} \underset{\boldsymbol{\beta}_n}{\text{maximize}} & \gamma_n \\ \text{subject to} & \gamma_n \leq \beta_{n,j} E_{n,j}, \quad \forall j \in \mathcal{M}, \\ & \sum\limits_{j \in \mathcal{M}} \beta_{n,j} \leq F, \\ & \sum\limits_{j \in \mathcal{M}} \beta_{n,j} E_{n,j} \leq E_n^{\text{back}} B, \end{cases} \tag{11}$$

where $\boldsymbol{\beta}_n = \{\beta_{n,j} | \forall j \in \mathcal{M}\}$ is the set of fronthaul spectrum allocations in time slot n and γ_n is an auxiliary variable. Then, the constraints (7b), (7c) and (7d) can be simplified as

$$R^{\text{out}}(x_n) \geq R_{\min}, \quad \forall n \in \mathcal{N}^+. \tag{12}$$

Moreover, the optimal solution of (11) can be derived in closed-form expression as

$$R^{\text{out}}(x_n) = \min\left\{ \frac{E_n^{\text{back}} B}{M}, \frac{F}{\sum_{j \in \mathcal{M}} \frac{1}{E_{n,j}}} \right\}, \tag{13}$$

where $M = |\mathcal{M}|$ is the number of users. Since $R^{\text{out}}(x_n)$ is non-smooth, we extend the constraints in (12) into the following two-part constraints for convenience.

$$\frac{E_n^{\text{back}} B}{M} \geq R_{\min}, \quad \forall n \in \mathcal{N}^+, \tag{14}$$

$$\frac{F}{\sum_{j \in \mathcal{M}} \frac{1}{E_{n,j}}} \geq R_{\min}, \quad \forall n \in \mathcal{N}^+. \tag{15}$$

The left-hand-side of (14) is a quasi-concave function with respect to x_n, and its superlevel set is a convex set [36]. Hence, (14) can be equivalently written as the following convex constraints

$$\|x_n - x^{\text{gbs}}\|^2 \leq \frac{\hat{K}^{\text{back}}}{\exp\left(\frac{R_{\min} M}{B}\right) - 1} - h^2, \quad \forall n \in \mathcal{N}, \tag{16}$$

where $\hat{K}^{\text{back}} = \frac{K^{\text{back}}/(4\pi f/c)^2}{\sigma}$. This is to say that the feasible set of $\boldsymbol{x}$ represented by (14) is a circle centered at the GBS.

To simplify the analysis, we empirically assume that the feasible set represented by (15) can be approximated by a circle centered at the geometric mean of user locations, where the geometric mean is denoted as $\bar{x}^{\text{user}} = \frac{\sum_{j \in \mathcal{M}} x_j^{\text{user}}}{M}$. The radius of the circle is obtained by doing a numerical root-finding of $\frac{F}{\sum_{j \in \mathcal{M}} \frac{1}{E_{n,j}}} - R_{\min}$ on the line $\mathcal{L} = \{\rho r + \bar{x}^{\text{user}} | \rho \in \mathbb{R}^+\}$, where $r = \frac{x^{\text{gbs}} - \bar{x}^{\text{user}}}{\|x^{\text{gbs}} - \bar{x}^{\text{user}}\|}$ [37].

Then, as shown in Fig. 3, the circular trajectory with the largest radius is obtained as the inscribed circle of the intersection of the feasible sets (14) and (15). The optimal velocity can be obtained by substituting the radius of the inscribed circle into (9).

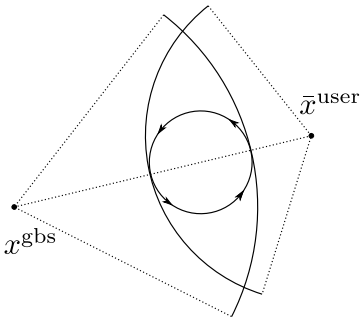

FIGURE 3. The circular trajectory for out-band backhaul.

B. SEQUENTIAL CONVEX OPTIMIZATION FOR OUT-BAND BACKHAUL

As shown in Fig. 3, the intersection of the feasible sets (14) and (15) is spindle-shaped, and the circular trajectory may not be the optimal trajectory. To further reduce energy consumption, a sequential convex optimization algorithm is developed to solve the trajectory design problem (7). In particular, the original problem is approximated by more tractable approximations on local points, and the local points are updated after each iteration.

Firstly, an upper bound of the energy consumption model (1) is given by

$$P \le \sum_{n\in\mathcal{N}} \left(c_1\|v_n\|^3 + \frac{c_2}{\|v_n\|}\left(1+\frac{\|a_n\|^2}{g^2}\right)\right) + \Delta\kappa \quad (17a)$$

$$\le \sum_{n\in\mathcal{N}} \left(c_1\|v_n\|^3 + \frac{c_2}{\|v_n\|} + \frac{c_2\|a_n\|^2}{g^2\|v_n\|}\right) + \Delta\hat{\kappa}, \quad (17b)$$

where $\Delta\hat{\kappa} = \frac{m}{2}\|v_N\|^2 - \frac{m}{2}\left(\|v_0^{(t)}\|^2 + 2(v_0^{(t)})^\mathsf{T}(v_0 - v_0^{(t)})\right)$ and $v_0^{(t)}$ is a local point obtained in the iteration t. (17a) is obtained by using the fact that $\frac{(a_n^\mathsf{T} v_n)^2}{\|v_n\|^2} \ge 0$. The upper bound in (17a) is tight when the acceleration direction is perpendicular to the velocity direction, i.e., $a_n^\mathsf{T} v_n = 0$. $\Delta\hat{\kappa}$ is obtained by applying the first order Taylor expansion of $\Delta\kappa$ with respect to v_0, and the inequality in (17b) is a result of the property that the Taylor expansion is a global upper estimator of a concave function.

By using (17b), the problem (7) is transformed into minimizing an upper bound of the energy consumption. Furthermore, by replacing the constraints (7b), (7c) and (7d) with (14) and (15), the problem in (7) is reformulated as

$$\underset{\boldsymbol{x},\boldsymbol{v},\boldsymbol{a},\boldsymbol{\tau},\boldsymbol{\epsilon}}{\text{minimize}} \ \delta \sum_{n\in\mathcal{N}} \left(c_1\|v_n\|^3 + \frac{c_2}{\tau_n} + \frac{c_2\|a_n\|^2}{g^2\tau_n}\right) + \Delta\hat{\kappa} \quad (18a)$$

$$\text{subject to } 0 \le \tau_n, \quad \forall n \in \mathcal{N}, \quad (18b)$$

$$\tau_n^2 \le \|v_n\|^2, \quad \forall n \in \mathcal{N}, \quad (18c)$$

$$\sum_{j\in\mathcal{M}} \frac{1}{\epsilon_{n,j}} \le \frac{F}{R_{\min}}, \quad \forall n \in \mathcal{N}^+, \quad (18d)$$

$$0 \le \epsilon_{n,j}, \ \forall j \in \mathcal{M}, \quad \forall n \in \mathcal{N}^+, \quad (18e)$$

$$\epsilon_{n,j} \le E_{n,j}, \quad \forall j \in \mathcal{M}, \ \forall n \in \mathcal{N}^+, \quad (18f)$$

$$(2), (3), (4), (5), (6) \text{ and } (16),$$

where $\boldsymbol{\tau} = \{\tau_n | \forall n \in \mathcal{N}\}$ and $\boldsymbol{e} = \{e_{n,j} | \forall j \in \mathcal{M}, \forall n \in \mathcal{N}^+\}$ are the auxiliary variables. It can be shown that $\tau_n = \|v_n\|, \forall n \in \mathcal{N}$ at the optimum of (18) since otherwise we can always increase τ_n to obtain a better objective value. Also, it can be shown that the constraints in (15) are equivalent to the combination of (18d), (18e) and (18f) since the right-hand-side of (18d) is minimized at $\epsilon_{n,j} = E_{n,j}, \forall n \in \mathcal{N}^+$. As a result of the reformulation, the objective function (18a) and the fronthaul spectrum efficiency constraints (18d) are now convex. The remaining non-convex parts of the problem (18) are the constraints (6), (18c) and (18f).

To tackle the remaining non-convexity in (18), the local approximations are derived. By taking the Taylor expansion of $\|v_n\|^2$ on v_n, the convex constraints that approximate (18c) are obtained as

$$\tau_n^2 \le \|v_n^{(t)}\|^2 + 2(v_n^{(t)})^\mathsf{T}(v_n - v_n^{(t)}), \quad \forall n \in \mathcal{N}, \quad (19)$$

where $v_n^{(t)}, n \in \mathcal{N}$ are local points obtained in the iteration t. Similarly, let $v_N^{(t)}$ be a local point, the constraint (6) can be approximated by

$$\|v_0\|^2 \le \|v_N^{(t)}\|^2 + 2(v_N^{(t)})^\mathsf{T}(v_N - v_N^{(t)}). \quad (20)$$

With regard to (18f), although $E_{n,j}$ is non-concave with respect to $x_{n,j}$, it is convex with respect to $d_{n,j}^2$. Thus, the approximation of (18f) is obtained by applying the Taylor expansion with respect to $d_{n,j}^2$ as

$$\epsilon_{n,j} \le \log\left(\frac{\hat{K}}{|d_{n,j}^{(t)}|^2} + 1\right) - \frac{\hat{K}\left(d_{n,j}^2 - |d_{n,j}^{(t)}|^2\right)}{|d_{n,j}^{(t)}|^2\left(|d_{n,j}^{(t)}|^2 + \hat{K}\right)}, \quad \forall j \in \mathcal{M}, \quad \forall n \in \mathcal{N}^+, \quad (21)$$

where $d_{n,j}^{(t)}$ is a local point and $\hat{K} = \frac{K/(4\pi f/c)^2}{\sigma}$. Since $d_{n,j}^2$ is convex in respect to x_n, the right-hand-side of (21) is concave with respect to x_n. Thus, the constraints in (21) is convex.

The problem (7) can now be approximated by a convex optimization model as follows.

$$\underset{\boldsymbol{x},\boldsymbol{v},\boldsymbol{a},\boldsymbol{\tau},\boldsymbol{\epsilon}}{\text{minimize}} \ \delta \sum_{n\in\mathcal{N}} \left(c_1\|v_n\|^3 + \frac{c_2}{\tau_n} + \frac{c_2\|a_n\|^2}{g^2\tau_n}\right) + \Delta\hat{\kappa}$$

$$\text{subject to } (2), (3), (4), (5) \text{ and } (16),$$

$$(18b), (18d), (18e), (19), (20) \text{ and } (21). \quad (22)$$

As a convex optimization problem, (22) can be solved effectively by a general propose convex problem solver [36], [38]. Then, the original non-convex problem (7) can be solved by iterative optimizing of (22) with the local points $v_n^{(t)}, \forall n \in \mathcal{N}^+$ and $d_{n,j}^{(t)}, \forall j \in \mathcal{M}, \forall n \in \mathcal{N}^+$ updated in each iteration, and the circular trajectory derived in Section III-A is used as the initial local points.

For the computational complexity of solving (22), the complexity analysis of the ellipsoid method is used since the ellipsoid method can provide a complexity upper bound for solving convex optimization problems [39]. The ellipsoid method can be viewed as a multi-dimensional extension of the bisection search, where the search area is cut in half in each iteration. More specifically, the complexity of $\mathcal{O}(MN)$ is required in each iteration to determine the multi-dimensional cut. Since the ellipsoid method takes the complexity of $\mathcal{O}(M^2N^2)$ to converge, the total complexity for solving (22) is $\mathcal{O}(M^3N^3)$.

Moreover, due to the non-convex nature of (18), it is difficult to analyze the convergence of the sequential convex optimization process theoretically. Instead, the corresponding experiments are conducted to demonstrate the convergence behavior in Section V.

IV. RESOURCE ALLOCATION AND TRAJECTORY DESIGN FOR IN-BAND BACKHAUL SCHEME

Under the in-band backhaul scheme, the fronthaul and backhaul resource allocations are no longer fixed parameters, but design variables that can be dynamically changed in different time slots. Let $\boldsymbol{F} = \{F_n | \forall n \in \mathcal{N}\}$ and $\boldsymbol{B} = \{B_n | \forall n \in \mathcal{N}\}$ be the set of spectrum allocation at different time slots for fronthaul and backhaul links, respectively. Given the total bandwidth C, the in-band backhaul optimization problem is formulated as

$$\begin{aligned}
\underset{\boldsymbol{F},\boldsymbol{B},\boldsymbol{\beta},\boldsymbol{x},\boldsymbol{v},\boldsymbol{a}}{\text{minimize}} \quad & P && \text{(23a)}\\
\text{subject to} \quad & R_{\min} \le \beta_{n,j} E_{n,j}, \quad \forall j \in \mathcal{M}, \forall n \in \mathcal{N}^+, && \text{(23b)}\\
& \sum_{j\in\mathcal{M}} \beta_{n,j} \le F_n, \quad \forall n \in \mathcal{N}^+, && \text{(23c)}\\
& \sum_{j\in\mathcal{M}} \beta_{n,j} E_{n,j} \le E_n^{\text{back}} B_n, \quad \forall n \in \mathcal{N}^+, && \text{(23d)}\\
& F_n + B_n \le C, \quad \forall n \in \mathcal{N}^+, && \text{(23e)}\\
& \text{(2), (3), (4), (5) and (6).}
\end{aligned}$$

The minimal rate requirement is enforced by the constraints in (23b), the fronthaul resource limitations and the backhaul rate limitations are represented by (23c) and (23d), respectively. In addition, the constraints in (23e) indicate that the total bandwidth used for fronthaul and backhaul links should not exceed the total available bandwidth.

A. CIRCULAR TRAJECTORY FOR IN-BAND BACKHAUL

Similar to the out-band backhaul scheme, an empirical method is developed in this subsection to obtain the circular trajectory with the maximum radius. In particular, $R^{\text{in}}(x_n)$ is defined as the max-min user rate, which is given as the optimal objective value of the following optimization problem.

$$R^{\text{in}}(x_n) = \left\{ \begin{aligned}
&\underset{\boldsymbol{\beta}_n}{\text{maximize}} \ \gamma_n\\
&\text{subject to} \ \gamma_n \le \beta_{n,j} E_{n,j}, \ \forall j \in \mathcal{M},\\
&\qquad \sum_{j\in\mathcal{M}} \beta_{n,j} \le F_n,\\
&\qquad \sum_{j\in\mathcal{M}} \beta_{n,j} E_{n,j} \le E_n^{\text{back}} B_n,\\
&\qquad F_n + B_n \le C.
\end{aligned} \right. \tag{24}$$

By using $R^{\text{in}}(x_n)$, the constraints of (23b), (23c), (23d) and (23e) can be replaced by

$$R_{\min} \le R^{\text{in}}(x_n), \quad \forall n \in \mathcal{N}^+. \tag{25}$$

Furthermore, the problem in (24) can be solved in closed-form expression as

$$R^{\text{in}}(x_n) = \frac{C}{\frac{M}{E_n^{\text{back}}} + \sum_{j\in\mathcal{M}} \frac{1}{E_{n,j}}}. \tag{26}$$

As we will see in Section V, the constraints in (25) can be approximated by an ellipse. As shown in Fig. 4, we empirically use the line $\mathcal{L}^a = \{\rho r_a + x^{\text{gbs}} | \rho \in \mathbb{R}\}$ as the major axis, where $r_a = \frac{x^{\text{gbs}} - \bar{x}^{\text{user}}}{\|x^{\text{gbs}} - \bar{x}^{\text{user}}\|}$ is the major axis direction. The length of the major axis is obtained by doing a root-finding of $\frac{C}{\frac{M}{E_n^{\text{back}}} + \sum_{j\in\mathcal{M}} \frac{1}{E_{n,j}}} - R^{\text{in}}(x_n)$ on $\mathcal{L}^a$ to locate the two vertexes of the ellipse. The ellipse center x_c is obtained as the midpoint of the two vertexes. Furthermore, the minor axis direction is obtained by rotating the major axis for 90°, i.e., $r_b = \begin{bmatrix} 0 & -1 \\ 1 & 0 \end{bmatrix} r_a$. The co-vertexes are obtained by doing another root-finding on line $\mathcal{L}^b = \{\rho r_b + x_c | \rho \in \mathbb{R}\}$. Finally, the circular trajectory is obtained as the inscribed circle of the ellipse. The corresponding optimal velocity is calculated by using (9).

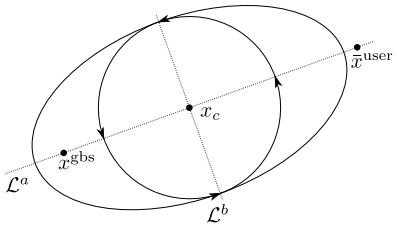

FIGURE 4. The circular trajectory for in-band backhaul.

B. SEQUENTIAL CONVEX OPTIMIZATION FOR IN-BAND BACKHAUL

By employing the upper bound of P in (17b) and the closed-form expression of $R^{\text{in}}(x_n)$ in (26), (23) can be reformulated as

$$\begin{aligned}
\underset{\substack{\boldsymbol{x},\boldsymbol{v},\boldsymbol{a},\boldsymbol{\tau}\\ \boldsymbol{\epsilon},\boldsymbol{\epsilon}^{\text{back}}}}{\text{minimize}} \quad & \delta \sum_{n\in\mathcal{N}} \left(c_1 \|v_n\|^3 + \frac{c_2}{\tau_n} + \frac{c_2 \|a_n\|^2}{g^2 \tau_n} \right) + \Delta\hat{\kappa} && \text{(27a)}\\
\text{subject to} \quad & 0 \le \epsilon_n^{\text{back}}, \quad \forall n \in \mathcal{N}^+, && \text{(27b)}\\
& \epsilon_n^{\text{back}} \le E_n^{\text{back}}, \quad \forall n \in \mathcal{N}^+, && \text{(27c)}\\
& \frac{M}{\epsilon_n^{\text{back}}} + \sum_{j\in\mathcal{M}} \frac{1}{\epsilon_{n,j}} \le \frac{C}{R_{\min}}, \quad \forall n \in \mathcal{N}^+, && \text{(27d)}\\
& \text{(2), (3), (4), (5) and (6),}\\
& \text{(18b), (18c), (18e) and (18f),}
\end{aligned}$$

where $\boldsymbol{\epsilon}^{\text{back}} = \{\epsilon_n^{\text{back}} | \forall n \in \mathcal{N}^+\}$ is a set of auxiliary variables. It can be proved that the combination of (18e), (18f), (27b), (27c) and (27d) is equivalent to (25). The remaining non-convexity parts of (27) are the constraints (6), (18c), (18f) and (27c).

Similar to (18), the non-convexity parts can be handled by using approximations based on local points. In addition to the approximations (19), (20) and (21) derived in Section III-B, the constraints in (27c) can be approximated by

$$\begin{aligned}
\epsilon_n^{\text{back}} \le & \log\left(\frac{\hat{K}^{\text{back}}}{|d_n^{\text{back},(t)}|^2} + 1 \right)\\
& - \frac{\hat{K}^{\text{back}} \left(|d_n^{\text{back}}|^2 - |d_n^{\text{back},(t)}|^2 \right)}{|d_n^{\text{back},(t)}|^2 \left(|d_n^{\text{back},(t)}|^2 + \hat{K} \right)}, \quad \forall n \in \mathcal{N}^+,
\end{aligned} \tag{28}$$

where $d_n^{\text{back},(t)}, n \in \mathcal{N}^+$ are local points obtained in the iteration t.

Finally, a convex optimization problem is formulated to approximate (23) as

$$\begin{aligned} \underset{\substack{\boldsymbol{x},\boldsymbol{v},\boldsymbol{a},\boldsymbol{\tau} \\ \epsilon,\epsilon^{\text{back}}}}{\text{minimize}} \quad & \delta \sum_{n\in\mathcal{N}} \left(c_1 \|v_n\|^3 + \frac{c_2}{\tau_n} + \frac{c_2 \|a_n\|^2}{g^2 \tau_n} \right) + \Delta\hat{\kappa} \\ \text{subject to} \quad & (2), (3), (4), (5), (18b), (18e), (19) \text{ and } (20), \\ & (21), (27b), (27d) \text{ and } (28). \end{aligned} \tag{29}$$

As a result, (23) can be solved by iteratively optimizing (29) with a convex problem solver [36], [38] and update the local points, where the circular trajectory is used as the initial local points.

The complexity analysis of problem (29) is similar to problem (22), and the total complexity is also $\mathcal{O}(M^3N^3)$. Moreover, the convergence behavior of the sequential convex optimization process for solving (27) is demonstrated in Section V.

V. SIMULATIONS RESULTS

In this section, the numerical results are provided to validate our proposed methods. In the simulations, $M = 50$ users are distributed in a square area of size 1 km × 1 km. Without loss of generality, it is assumed that the coordinate of the GBS is (0, 0). A fixed-wing UBS is deployed to provide continuous available wireless services to the users. Other simulation parameters are listed in Table 1.

TABLE 1. Simulation parameters.

Symbols	Value	Description
h	100 m	Altitude of the UBS
g	9.8 m/s^2	Gravitational acceleration
f	2 GHz	Fronthaul carrier Frequency
f^{back}	2 GHz	Backhaul carrier Frequency
K	30 dBm	UBS transmit power
K^{back}	30 dBm	GBS transmit power
σ	−100 dBm	Noise power
m	10 kg	The mass of UBS
c_1	9.26×10^{-4} kg/m	Energy consumption parameter
c_2	2250 kg m^3/s^4	Energy consumption parameter
C	20 MHz	In-band total bandwidth
F	10 MHz	Out-band fronthaul bandwidth
B	10 MHz	Out-band backhaul bandwidth
T	100 s	UBS fly time duration
N	100	Number of discrete time slots
δ	1 s	Time slot duration

Fig. 5 plots the max-min user rate at different UBS locations under both out-band and in-band schemes, where the bright color indicates the high values and the dark color indicates the low values. The contour lines that indicate different max-min rates are also illustrated to emphasize the feasible sets of different required rates. The location of GBS is marked as red dots in the figures. It is observed that the feasible set enlarges with the decreasing of the required rates. This is intuitive since the corresponding constraints are relaxed when $R_{\min}$ is decreased. Also, the feasible set of the in-band

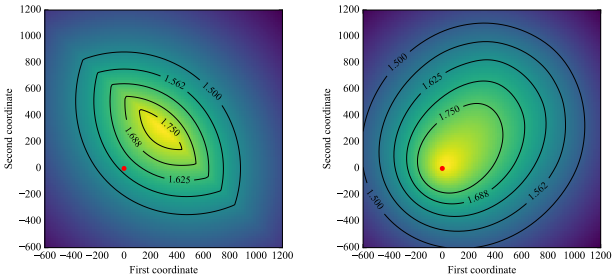

(a) Out-band backhaul. (b) In-band backhaul.

FIGURE 5. Max-min rate for different backhaul schemes (Mnat/s).

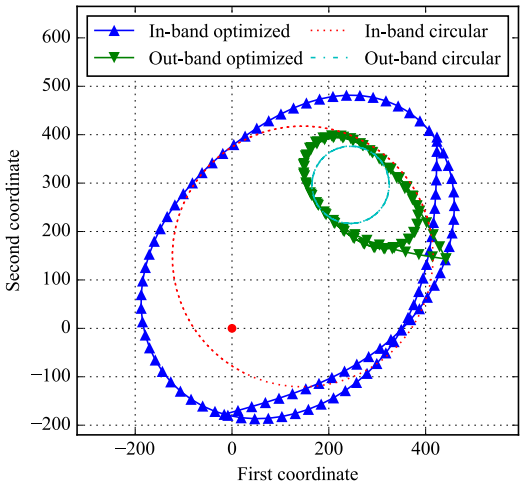

FIGURE 6. Trajectory comparison of in-band and out-band backhaul.

backhaul scheme is significantly larger than the feasible set of the out-band backhaul scheme with the same required rate. This is a result of the higher spectrum utilization achieved by the in-band backhaul since the resource allocation for fronthaul and backhaul can be dynamically adjusted. More specifically, when the UBS flies away from the users, more resources are allocated to the fronthaul to compensate for the long-distance transmission, and vise versa.

Fig. 6 plots the optimized trajectories of both out-band and in-band backhaul schemes under the required minimum rate of $R_{\min} = 1.75$Mnat/s, where the location of GBS is illustrated as a red dot. The corresponding circular trajectories are also illustrated for comparison. As shown in Fig. 6, the optimized trajectories are different from the circular trajectories. By comparing the optimized trajectories with the contour lines in Fig. 5, it is observed that the trajectories are adapted into the shapes of feasible sets to reduce maneuvers, which in turn reduce the energy consumption. Especially, instead of following the contour line, the optimized trajectory for out-band backhaul scheme follows a smooth curve around the sharp corners of the spindle-shaped feasible set to avoid the sharp turning.

Fig. 7 plots the energy consumption of the optimized trajectories under different required minimum rate and different backhaul schemes. The energy consumption of the circular trajectories are also illustrated as benchmarks. It is observed in Fig. 7 that a significant improvement is achieved by the

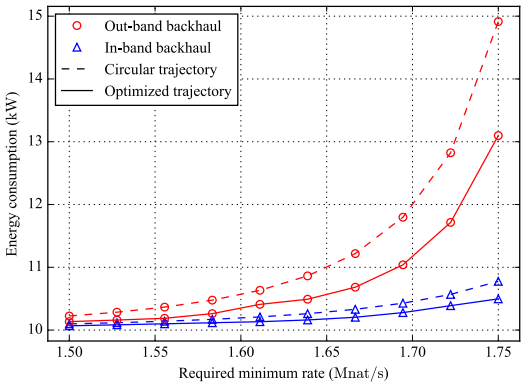

FIGURE 7. Energy consumption with different backhaul schemes and different minimum required rates.

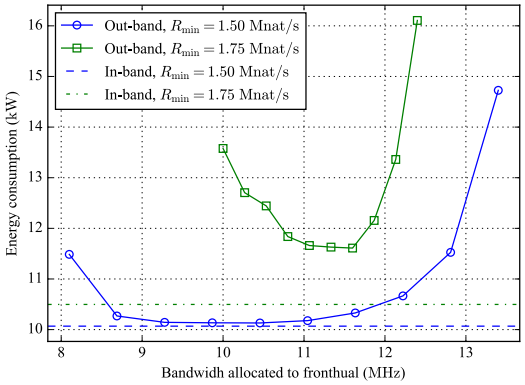

FIGURE 8. Energy Consumption with different separation of spectrum resources.

optimized trajectories compared with the circular trajectories. This is a result of adapting the trajectories to the feasible sets that unnecessary maneuvers are avoided. It is also shown that the energy consumption increases with the required minimum rate. By comparing the feasible sets under different required rates in Fig. 5, this result becomes intuitive that the increased minimum rate would result in smaller feasible sets, and additional energy consumption is required to keep the UBS from leaving the feasible set. For a similar reason, as demonstrated in Fig. 7, the in-band backhaul scheme can achieve a lower energy consumption compared with the out-band backhaul.

Fig. 8 plots optimized energy consumption of out-band backhaul scheme under different required minimum rate and different fronthaul/backhaul resource allocations. The optimization results of the in-band backhaul scheme are also illustrated as a reference. The feasible sets are already very small at the boundaries of the illustrated curves that the optimization problem would become infeasible if the resources allocated to fronthaul is further increased or reduced. As shown in Fig. 8, a suitable fronthaul/backhaul resource allocation can significantly reduce energy consumption. However, as a result of the dynamic fronthaul/backhaul resource allocation, the in-band backhaul scheme would outperform the optimal resource allocation in the out-band backhaul scheme.

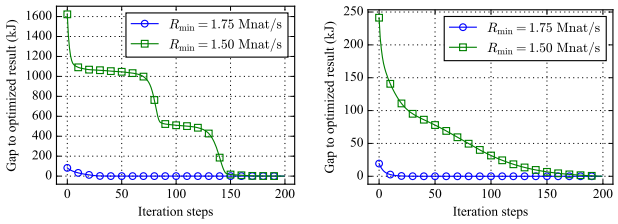

(a) Out-band backhaul. (b) In-band backhaul.

FIGURE 9. Converge behavior for different backhaul schemes.

Fig. 9 plots the converge behavior of both out-band and in-band backhaul schemes. As shown in the figures, when the required minimum rate is $R_{\min} = 1.50$ Mnat/s, the energy consumption gaps between the circular trajectories and optimized trajectories are small, and our proposed algorithm converged within about 10 steps. The gaps are much larger when $R_{\min} = 1.75$ Mnat/s, and the convergence takes more steps. However, an optimized result can still be achieved within 200 steps. More interestingly, the convergence curve of out-band backhaul with $R_{\min} = 1.75$ Mnat/s has two flat areas before the final convergence. This convergence behavior reflect the non-convex nature of the energy-efficient optimization problem.

VI. CONCLUSION

In this paper, we propose a joint fixed-wing UBS trajectory and resource allocation scheme that can guarantee a continuous available minimum rate for each user at all times. The resource allocation is derived in closed-form for both the out-band and in-band backhaul schemes. Then, a sequential convex optimization framework is proposed to solve the energy-efficient UBS trajectory design problems. Moreover, we provide detailed evaluations of our proposed methods. It is shown that our proposed methods can achieve significant lower energy consumption than the circular trajectory scheme. Besides, we demonstrated that the in-band backhaul scheme could achieve lower energy consumption than the out-band backhaul scheme.

REFERENCES

[1] I. Bor-Yaliniz and H. Yanikomeroglu, "The new frontier in RAN heterogeneity: Multi-tier drone-cells," *IEEE Commun. Mag.*, vol. 54, no. 11, pp. 48–55, Nov. 2016.
[2] Y. Zeng, R. Zhang, and T. J. Lim, "Wireless communications with unmanned aerial vehicles: Opportunities and challenges," *IEEE Commun. Mag.*, vol. 54, no. 5, pp. 36–42, May 2016.
[3] S. Sekander, H. Tabassum, and E. Hossain, "Multi-tier drone architecture for 5G/B5G cellular networks: Challenges, trends, and prospects," *IEEE Commun. Mag.*, vol. 56, no. 3, pp. 96–103, Mar. 2018.
[4] F. Ono, H. Ochiai, and R. Miura, "A wireless relay network based on unmanned aircraft system with rate optimization," *IEEE Trans. Wireless Commun.*, vol. 15, no. 11, pp. 7699–7708, Nov. 2016.
[5] P. Yang, X. Cao, C. Yin, Z. Xiao, X. Xi, and D. Wu, "Proactive drone-cell deployment: Overload relief for a cellular network under flash crowd traffic," *IEEE Trans. Intell. Transp. Syst.*, vol. 18, no. 10, pp. 2877–2892, Oct. 2017.
[6] E. Kalantari, H. Yanikomeroglu, and A. Yongacoglu, "On the number and 3D placement of drone base stations in wireless cellular networks," in *Proc. IEEE 84th Veh. Technol. Conf. (VTC-Fall)*, Montreal, QC, Canada, Sep. 2016, pp. 1–6.

[7] S. Chandrasekharan, K. Gomez, A. Al-Hourani, S. Kandeepan, T. Rasheed, L. Goratti, L. Reynaud, D. Grace, I. Bucaille, T. Wirth, and S. Allsopp, "Designing and implementing future aerial communication networks," *IEEE Commun. Mag.*, vol. 54, no. 5, pp. 26–34, May 2016.
[8] K. Li, W. Ni, X. Wang, R. P. Liu, S. S. Kanhere, and S. Jha, "Energy-efficient cooperative relaying for unmanned aerial vehicles," *IEEE Trans. Mobile Comput.*, vol. 15, no. 6, pp. 1377–1386, Jun. 2016.
[9] X. Sun and N. Ansari, "Jointly optimizing drone-mounted base station placement and user association in heterogeneous networks," in *Proc. IEEE Int. Conf. Commun. (ICC)*, Kansas City, MO, USA, May 2018, pp. 1–6.
[10] N. Wang, E. Hossain, and V. K. Bhargava, "Joint downlink cell association and bandwidth allocation for wireless backhauling in two-tier HetNets with large-scale antenna arrays," *IEEE Trans. Wireless Commun.*, vol. 15, no. 5, pp. 3251–3268, May 2016.
[11] A. Al-Hourani, S. Kandeepan, and S. Lardner, "Optimal LAP altitude for maximum coverage," *IEEE Wireless Commun. Lett.*, vol. 3, no. 6, pp. 569–572, Dec. 2014.
[12] R. I. Bor-Yaliniz, A. El-Keyi, and H. Yanikomeroglu, "Efficient 3-D placement of an aerial base station in next generation cellular networks," in *Proc. IEEE Int. Conf. Commun. (ICC)*, Kuala Lumpur, Malaysia, May 2016, pp. 1–5.
[13] J. Lyu, Y. Zeng, R. Zhang, and T. J. Lim, "Placement optimization of UAV-mounted mobile base stations," *IEEE Commun. Lett.*, vol. 21, no. 3, pp. 604–607, Mar. 2017.
[14] M. Mozaffari, W. Saad, M. Bennis, and M. Debbah, "Optimal transport theory for power-efficient deployment of unmanned aerial vehicles," in *Proc. IEEE Int. Conf. Commun. (ICC)*, Kuala Lumpur, Malaysia, May 2016, pp. 1–6.
[15] M. Mozaffari, W. Saad, M. Bennis, and M. Debbah, "Wireless communication using unmanned aerial vehicles (UAVs): Optimal transport theory for hover time optimization," *IEEE Trans. Wireless Commun.*, vol. 16, no. 12, pp. 8052–8066, Dec. 2017.
[16] Y. Chen, W. Feng, and G. Zheng, "Optimum placement of UAV as relays," *IEEE Commun. Lett.*, vol. 22, no. 2, pp. 248–251, Feb. 2018.
[17] W. Shi, J. Li, W. Xu, H. Zhou, N. Zhang, S. Zhang, and X. Shen, "Multiple drone-cell deployment analyses and optimization in drone assisted radio access networks," *IEEE Access*, vol. 6, pp. 12518–12529, 2018.
[18] C. Qiu, Z. Wei, Z. Feng, and P. Zhang, "Joint resource allocation, placement and user association of multiple UAV-mounted base stations with in-band wireless backhaul," *IEEE Wireless Commun. Lett.*, vol. 8, no. 6, pp. 1575–1578, Dec. 2019.
[19] X. Yuan, Z. Feng, W. Xu, W. Ni, J. A. Zhang, Z. Wei, and R. P. Liu, "Capacity analysis of UAV communications: Cases of random trajectories," *IEEE Trans. Veh. Technol.*, vol. 67, no. 8, pp. 7564–7576, Aug. 2018.
[20] Y. Zeng, R. Zhang, and T. J. Lim, "Throughput maximization for UAV-enabled mobile relaying systems," *IEEE Trans. Commun.*, vol. 64, no. 12, pp. 4983–4996, Dec. 2016.
[21] Q. Wu, Y. Zeng, and R. Zhang, "Joint trajectory and communication design for multi-UAV enabled wireless networks," *IEEE Trans. Wireless Commun.*, vol. 17, no. 3, pp. 2109–2121, Mar. 2018.
[22] Y. Sun, D. Xu, D. W. K. Ng, L. Dai, and R. Schober, "Optimal 3D-trajectory design and resource allocation for solar-powered UAV communication systems," *IEEE Trans. Commun.*, vol. 67, no. 6, pp. 4281–4298, Jun. 2019.
[23] Y. Cai, Z. Wei, R. Li, D. Wing Kwan Ng, and J. Yuan, "Energy-efficient resource allocation for secure UAV communication systems," 2019, *arXiv:1901.09308*. [Online]. Available: http://arxiv.org/abs/1901.09308
[24] Q. Wu, L. Liu, and R. Zhang, "Fundamental trade-offs in communication and trajectory design for UAV-enabled wireless network," *IEEE Wireless Commun.*, vol. 26, no. 1, pp. 36–44, Feb. 2019.
[25] Q. Wu and R. Zhang, "Common throughput maximization in UAV-enabled OFDMA systems with delay consideration," *IEEE Trans. Commun.*, vol. 66, no. 12, pp. 6614–6627, Dec. 2018.
[26] D. W. Matolak and R. Sun, "Air–Ground channel characterization for unmanned aircraft Systems—Part III: The suburban and near-urban environments," *IEEE Trans. Veh. Technol.*, vol. 66, no. 8, pp. 6607–6618, Aug. 2017.
[27] B. V. Der Bergh, A. Chiumento, and S. Pollin, "LTE in the sky: Trading off propagation benefits with interference costs for aerial nodes," *IEEE Commun. Mag.*, vol. 54, no. 5, pp. 44–50, May 2016.
[28] X. Lin, V. Yajnanarayana, S. D. Muruganathan, S. Gao, H. Asplund, H.-L. Maattanen, M. Bergstrom, S. Euler, and Y.-P.-E. Wang, "The sky is not the limit: LTE for unmanned aerial vehicles," *IEEE Commun. Mag.*, vol. 56, no. 4, pp. 204–210, Apr. 2018.
[29] *Enhanced LTE support for Aerial Vehicles*," 3rd Generation Partnership Project, 3GPP, document TR 36.777, 2017.
[30] D. W. Matolak and R. Sun, "Air–ground channel characterization for unmanned aircraft systems—Part I: Methods, measurements, and models for over-water settings," *IEEE Trans. Veh. Technol.*, vol. 66, no. 1, pp. 26–44, Jan. 2017.
[31] J. Zhang, Y. Zeng, and R. Zhang, "UAV-enabled radio access network: Multi-mode communication and trajectory design," *IEEE Trans. Signal Process.*, vol. 66, no. 20, pp. 5269–5284, Oct. 2018.
[32] J. Hoydis, K. Hosseini, S. Ten Brink, and M. Debbah, "Making smart use of excess antennas: Massive MIMO, small cells, and TDD," *Bell Labs Tech. J.*, vol. 18, no. 2, pp. 5–21, Sep. 2013.
[33] C. D. Franco and G. Buttazzo, "Energy-aware coverage path planning of UAVs," in *Proc. IEEE Int. Conf. Auto. Robot Syst. Competitions*, Vila Real, Portugal, Apr. 2015, pp. 111–117.
[34] C. Desset, B. Debaillie, V. Giannini, A. Fehske, G. Auer, H. Holtkamp, W. Wajda, D. Sabella, F. Richter, M. J. Gonzalez, H. Klessig, I. Godor, M. Olsson, M. A. Imran, A. Ambrosy, and O. Blume, "Flexible power modeling of LTE base stations," in *Proc. IEEE Wireless Commun. Netw. Conf. (WCNC)*, Shanghai, China, Apr. 2012, pp. 2858–2862.
[35] Y. Zeng and R. Zhang, "Energy-efficient UAV communication with trajectory optimization," *IEEE Trans. Wireless Commun.*, vol. 16, no. 6, pp. 3747–3760, Jun. 2017.
[36] S. Boyd and L. Vandenberghe, *Convex Optimization*. Cambridge, U.K.: Cambridge Univ. Press, 2004.
[37] W. H. Press, S. A. Teukolsky, W. T. Vetterling, and B. P. Flannery, *Numerical Recipes: The Art of Scientific Computing*, 3rd ed. New York, NY, USA: Cambridge Univ. Press, 2007.
[38] A. Wächter and L. T. Biegler, "On the implementation of an interior-point filter line-search algorithm for large-scale nonlinear programming," *Math. Program.*, vol. 106, no. 1, pp. 25–57, Mar. 2006, doi: 10.1007/s10107-004-0559-y.
[39] A. Ben-Tal and A. S. Nemirovskiaei, *Lectures on Modern Convex Optimization: Analysis, Algorithms, and Engineering Applications*. Philadelphia, PA, USA: Society for Industrial and Applied Mathematics, 2001.

CHEN QIU (Student Member, IEEE) received the B.E. degree from the Beijing University of Posts and Telecommunications (BUPT), Beijing, China, and the Queen Mary University of London, London, U.K., in 2013. He is currently pursuing the Ph.D. degree with BUPT. From 2015 to 2016, he was with the Department of Electrical and Computer Engineering, Texas A&M University. He was a Visiting Scholar with the Department of Electrical and Computer Engineering, University of California at Davis, from 2016 to 2017. His research interests include unmanned aerial vehicle-assisted wireless networks, wireless data analysis, and machine learning in wireless systems.

ZHIQING WEI (Member, IEEE) received the B.E. and Ph.D. degrees from the Beijing University of Posts and Telecommunications (BUPT), in 2010 and 2015, respectively. He is currently an Associate Professor with BUPT. He has published one book, three book chapters, and more than 50 articles. His research interests include the performance analysis and optimization of mobile ad hoc networks. He received the Exemplary Reviewer of the IEEE Wireless Communications Letters, in 2017, and the Best Paper Award of the International Conference on Wireless Communications and Signal Processing (WCSP), in 2018. He was the Registration Co-Chair of the IEEE/CIC International Conference on Communications in China (ICCC), in 2018, and the Publication Co-Chair of the IEEE/CIC ICCC, in 2019.

ZHIYONG FENG (Senior Member, IEEE) received the B.S., M.S., and Ph.D. degrees from the Beijing University of Posts and Telecommunications, China. She is currently a Professor and the Director of the Key Laboratory of Universal Wireless Communications, Ministry of Education, BUPT, China. Her main research interests include the wireless network virtualization in fifth-generation mobile networks (5G), spectrum sensing and dynamic spectrum management in cognitive wireless networks, universal signal detection and identification, network information theory, and so on. She is active in standards development, such as ITU-R WP5A/WP5D, the IEEE 1990, ETSI, and CCSA.

PING ZHANG (Fellow, IEEE) received the M.S. degree in electrical engineering from Northwestern Polytechnical University, Xi'an, China, in 1986, and the Ph.D. degree in electric circuits and systems from the Beijing University of Posts and Telecommunications (BUPT), Beijing, China, in 1990. He is currently a Professor with BUPT. His research interests include cognitive wireless networks, fourth-generation mobile communication, fifth-generation mobile networks, communications factory test instruments, universal wireless signal detection instruments, and the mobile Internet. He was a recipient of the First and Second Prizes from the National Technology Invention and Technological Progress Awards and the First Prize Outstanding Achievement Award of Scientific Research in College. He is currently the Executive Associate Editor-in-Chief on information sciences of the *Chinese Science Bulletin*, a Guest Editor of the *IEEE Wireless Communications Magazine*, and an Editor of *China Communications*.